Urinary Sodium Wasting and Disrupted Collecting Duct Function in Mice with dRTA-Causing *SLC4A1* Mutations

Priyanka Mungara[1,2], Kristina MacNaughton[1,2], AKM Shahid Ullah,[1,2], Grace Essuman[1,2], Forough Chelangarimiyandoab[1,2], Rizwan Mumtaz[4], J. Christopher Hennings[4], Christian A. Hübner[4,5], Dominique Eladari[6,7,8], R. Todd Alexander[1,2,3], Emmanuelle Cordat[1,2*]

[1]Department of Physiology, University of Alberta, Edmonton, AB, Canada
[2]Membrane Protein Disease Research Group, University of Alberta, Edmonton, AB, Canada
[3]Department of Pediatric, University of Alberta, Edmonton, AB, Canada
[4]Institute of Human Genetics, Jena University Hospital, Friedrich Schiller University, Jena, Germany
[5] Center for rare diseases, Jena University Hospital, Friedrich Schiller University, Jena, Germany
[6]Service de Médecine de Précision des Maladies Rénales et Métaboliques, CHU Amiens Picardie ; Faculté de Médecine d'Amiens, Université de Picardie Jules Verne, Amiens, France
[7]Institut National de la Santé et de la Recherche Médicale U970, Centre de recherche PARCC (Paris centre de recherche cardiovasculaire), Paris, France
[8]French Clinical Research Infrastructure Network (F-CRIN): INI-CRCT, Vandœuvre-lès-Nancy, France

*To whom correspondence should be addressed: Department of Physiology, Membrane Protein Disease Research Group, Room 7-34, Medical Sciences Building, University of Alberta, Edmonton, Alberta, T6G 2H7, Canada, Tel: 780-492-0209, Fax : 780-492-8915, e-mail : cordat@ualberta.ca

Abstract

Distal renal tubular acidosis (dRTA) results in metabolic acidosis due to impaired urinary acidification and can also result in an unexplained urinary sodium-wasting phenotype. Here, we report the generation and characterization of a novel dRTA mutant mouse line, Ae1 L919X knockin (KI). Homozygous L919X KI mice exhibit typical dRTA features including a reduced ability to acidify urine in response to an acid load. This renal acidification defect was associated with a reduced number of Ae1-positive type A intercalated cells. To assess whether these mice exhibit urinary sodium-wasting as seen in some dRTA patients, homozygous KI L919X and the previously described R607H KI mice were fed a salt-depleted acid diet. In line with human patients, both mouse strains exhibited urinary sodium loss. Additionally, we identified increased expression of tight junction proteins claudin-4 and -10b, suggesting a compensatory paracellular pathway in the loop of Henle. Consistent with data from human patients, L919X KI mice displayed a milder phenotype than R607H KI mice. Our findings reveal that both mouse strains are appropriate models for dRTA with a urinary salt-wasting phenotype and a compensatory up-regulation of the paracellular pathway in the ascending limb of the loop of Henle.

Introduction

Renal tubular acidosis is a group of disorders in which dysregulation of acid-base homeostasis occurs due to improper bicarbonate reabsorption or non-volatile acid excretion by the nephron [1–5]. The inherited or acquired distal renal tubular acidosis (dRTA) impairs distal proton secretion and consequently renal acid excretion[2,4,6–9]. In addition to alkaline urine, patients with this disease can present hyperchloremic metabolic acidosis [2,5–9,11], hypokalemia[10], nephrocalcinosis / kidney stones[11], and renal sodium-wasting[12] with urinary-concentrating defects[5]. Notably, in some patients with inherited dRTA, correction of the metabolic acidosis does not prevent the renal sodium wasting and impaired renal salt handling, consistent with an ion tubular nephropathy[12].

dRTA affects the collecting duct (CD), a primary regulator of acid base homeostasis and electrolyte and fluid status, which finetunes the final urine composition[6]. The CD is composed of principal (PCs) and intercalated (ICs) cells. PCs mediate electrogenic salt and water reabsorption via the epithelial sodium channel (ENaC) and aquaporin 2 (AQP2)[13,14]. ICs regulate acid-base homeostasis via type A (A-ICs) and type B (B-IC)[15]. A-ICs secrete protons via an apical vacuolar proton ATPase (V-ATPase) and promote reabsorption of bicarbonate via the basolateral kidney anion exchanger 1 (kAE1). B-ICs facilitate bicarbonate secretion through the apical chloride/bicarbonate exchanger pendrin and reabsorb protons via a basolateral V-ATPase. The B-ICs also contribute to electroneutral salt reabsorption through the coupled activity of pendrin and the sodium-dependent chloride/bicarbonate exchanger (NDCBE)[16–18]. At least another intercalated cell type exists, characterized by apical expression of both pendrin and the V-ATPase, which is called non-A non-B ICs. The role of non-A, non-B cells is unclear.

Inherited dRTA may arise from autosomal dominant or recessive mutations in the *SLC4A1* gene encoding kAE1[19–22]. One such dominant mutation is the AE1 R589H, which is located on the cytosolic side of transmembrane domain 6 in the gate domain of kAE1[23–25]. *In vitro* studies have revealed retention in the endoplasmic reticulum[22,26] and apical mistargeting[27] of the mutant protein, and a 20-50 % reduction in its anion exchange activity compared to wild-type (WT) kAE1[22]. However, the mutant protein is able to hetero-oligomerize with WT kAE1[26,28], thereby resulting in a slightly reduced chloride/bicarbonate exchange at the cell surface. AE1 R901X is another common autosomal dominant mutation, which causes a cytosolic C-terminal tail truncation. In *in vitro* studies, the R901X mutant has normal transport activity, but is retained intracellularly and/or apically mistargeted[26,28–30], similarly to the R589H mutant. However, i*n vivo* data from transgenic

88 mice[31,32] and from dRTA patients' kidney biopsies[33,34] indicate that dRTA-causing variants
89 of kAE1 decrease the abundance of kAE1-positive ICs, emphasizing the limitations of *in*
90 *vitro* approaches. The kAe1 R607H knock in (KI) mouse model (orthologous to human
91 dRTA R589H mutation) recapitulates classical metabolic acidosis[31]. In this model, R607H
92 KI/KI mice exhibited proper kAe1 basolateral membrane targeting but decreased staining
93 intensity for both kAe1 and the B1 subunit of V-ATPase, and decreased Ae1 mRNA and
94 protein abundance. In addition, the remaining ICs of these mutant mice were larger in
95 size and accumulated the autophagy marker p62. Together, these results are consistent
96 with a reduced number of kAE1 positive A-ICs in the R607H KI/KI mice[31].
97
98 To date, the R607H KI mouse is the only dominant mouse model available. In the
99 current work, we report the generation and characterization of a second dRTA mutant
100 mouse model, carrying the autosomal dominant L919X KI mutation, orthologous to the
101 dominant R901X dRTA human mutation. This second mouse model exhibits the same
102 inability to acidify urine at baseline as the R607H KI mouse line[31], but overall has a milder
103 phenotype. Additionally, after salt restriction in acid-loaded mice, we found that both
104 L919X KI/KI and R607H KI/KI mice display a persistent urinary sodium loss as seen in
105 dRTA patients. The objectives of this work were to 1) characterize the kAe1 L919X KI
106 mouse line, 2) determine whether the two mouse models accurately reflect the urinary
107 ion loss seen in dRTA patients, and 3) begin investigating the mechanism causing urinary
108 sodium loss in these kAe1 mutant transgenic mice.
109
110
111

112 **Concise Methods**
113
114 *Generation of the L919X KI mice.* In Germany, animal experiments were approved by the
115 Thüringer Landesamt für Verbraucherschutz (TLV) under the license 02-016/14. In
116 Canada, animal protocols were approved by the University of Alberta's Animal Care and
117 Use Committee (AUP #1277) and were in accordance with the National and institutional
118 Animal care guidelines. L919X KI mice were generated by homologous recombination
119 similar to Ae1 R607H KI mice[33] as described in Supplemental Material.
120
121 *Metabolic Cage Experimental Design and Urine and Serum Analysis* R607H or L919X
122 mice and WT littermates were provided a "24 hour Salt Depletion or a "14 day Salt
123 Depletion with Acid Load" and placed in metabolic cages (Tecniplast) as described in
124 Supplemental Material. Body weight, chow and water consumption, urine (under mineral
125 oil), and feces were collected every 24 hours. Urine and serum analysis was completed
126 using i-STAT Chem8+ cartridge chip (Abbott Laboratories) and ion chromatography
127 (Dionex Aquion Ion Chromatography System, Thermo Fisher Scientific Inc.).
128
129 *Whole Kidney Tissues Analysis.* Immediately after collection, a half kidney was either
130 incubated in RNAlater (ThermoFisher) to use for reverse transcription quantitative PCR
131 or a quarter of kidney was decapsulated and processed for immunoblotting as described
132 in Supplemental Material (**Supplementary Tables 1 & 2**). Alternatively, kidneys
133 retrogradely perfused with PFA (4 %) were flash frozen in liquid nitrogen cooled
134 isopentane, and cryosections processed for Masson-Goldner stain, Von Kossa staining
135 or further processed for immunostaining as detailed in the Supplemental Material.
136
137 Detailed methods are listed in the Supplemental Material.
138
139

Results

Generation of Ae1 L919X Knock in Mice and Confirmation of Decreased numbers of A-ICs.

We generated mice carrying the orthologous mouse Ae1 L919X mutation by homologous recombination (**Figure 1 A**). Homozygous mice were viable, developed normally and were fertile. Neither gross kidney malformations nor nephrocalcinosis were observed (**Supplementary Figure 1 A & B**), similar to the Ae1 R607H mutant mice[33]. RT-qPCR analysis on whole kidneys from WT and L919X KI/KI mice at steady state confirmed a significant decrease in Ae1 mRNA abundance in the mutant animals (**Figure 1 B**). Immunostaining for kAe1 in the cortex and medulla of WT, heterozygous, and homozygous L919X KI mice (**Figure 1 C & D**) revealed that similar to WT mice, the kAe1 protein predominantly localized to the basolateral membrane, indicating normal membrane targeting of the mutant protein with no evidence of apical localization (**Figure 1 C**). This finding is also consistent with previous findings for R607H KI mice[31]. Additionally, staining intensity of kAe1 in L919X KI/KI mice was markedly reduced compared to WT and heterozygous L919X KI mice, both in the cortex and the medulla. Conversely, signals for pendrin did not exhibit genotype-dependent differences (**Figure 1 C & D**). Collectively, these results suggest a diminished abundance of kAE1-positive A-ICs in the L919X KI mouse model, consistent with Ae1 R607H KI mice observations.

L919X KI/KI and R607H KI/KI mice excrete an alkaline urine coupled with less urinary ammonium than WT littermates.

To validate the L919X KI/KI mice as a model of human dRTA, we assessed plasma and urine parameters at baseline (**Figure 2, Supplementary Table 3).** L919X KI/KI mice had alkaline urine compared to WT littermates (**Figure 2 A).** In agreement, they also excreted significant less urinary ammonium (**Figure 2 B**). Therefore, the Ae1 L919X KI mice display the characteristic inability to properly acidify urine as seen in dRTA human patients[5]. There was no difference in urine osmolality between genotypes (**Figure 2 C)** and the L919X KI/KI mice excreted sodium, chloride, and potassium comparably to WT mice (**Figure 2 D - F).** There were no differences in plasma ion concentrations or pH in the L919X KI/KI compared to WT mice, although both mouse lines had low plasma bicarbonate and pH, likely due to anesthesia (**Supplementary Table 3).** We completed a baseline analysis of the R607H KI/KI mice as well (**Figure 2 G-L and Supplementary Table 4**). We confirmed that R607H KI/KI mice displayed the same phenotype as L919X KI/KI mice at baseline (**Figure 2 G - L)**. These mutant mice had alkaline urine and

176 decreased ammonium excretion (**Figure 2 G, H),** as previously shown[33]. There was no
177 difference in urine osmolality (**Figure 2 I**) and mutant mice also excreted sodium, chloride,
178 and potassium to a similar extent as WT mice (**Figure 2 J - L)**. Overall, this baseline
179 characterization supports an abnormal urinary acidification in both dRTA mouse lines at
180 baseline, consistent with the hallmark characteristics of human dRTA patients[1].
181
182 *Acute sodium depletion confirms impaired urinary acidification and potassium excretion*
183 *in dRTA mutant mice compared to WT.*
184 To assess whether dRTA mutant mice show a salt-losing phenotype similar to
185 dRTA patients, we challenged R607H KI/KI, L919X KI/KI mice or WT littermates with a
186 sodium and chloride-depleted diet for 24 hours (**Protocol 1***)* (**Supplementary Figure 2,**
187 **Supplementary Tables 5 & 6**). Both L919X and R607H KI/KI mice consistently excreted
188 urine with a higher pH compared to WT littermates (**Supplementary Figure 2 A & F**).
189 Both mutant mice strains had no significant differences in urine osmolality between
190 genotypes, although there was trend towards lower osmolality for L919X KI/KI mice
191 (**Supplementary Figure 2 B & G).** Both L919X KI/KI and R607H KI/KI mice reduced
192 urinary sodium and chloride excretion appropriately, to a similar extent as WT littermates
193 (**Supplementary Figure 2 C-D, H-I**). Interestingly, L919X KI/KI mice excreted less urinary
194 potassium while there was only a trend in R607H KI/KI mice (**Supplementary Figure 2**
195 **E, J**). No significant plasma difference was found between genotypes for each strain,
196 except that R607H KI/KI mice continued to have increased plasma potassium compared
197 to WT littermates (**Supplementary Tables 5 & 6**). Together these results provide
198 preliminary evidence of renal electrolyte mishandling under acute sodium-depleted
199 conditions for both L919X and R607H KI/KI mice, suggesting a defective coupling of
200 potassium secretion to sodium and chloride reabsorption in the CDs of both strains.
201
202 *Salt depleted acid loading results in hypernatremia and hyperchloremia, as well as*
203 *increased renin levels in both dRTA mutant strains.*
204 To further challenge the dRTA mutant mice, we fed WT and mutant mice a sodium-
205 depleted acid diet (Supplementary Material, **Protocol 2***)*. This diet was designed to
206 recreate a study by Sebastien et al. revealing an urinary sodium wasting phenotype in
207 some dRTA patients on a salt-restricted diet for 8-10 days[12]. Following this challenge,
208 only R607H KI/KI mice displayed metabolic acidosis from the acid load, with decreased
209 plasma bicarbonate and pH (**Supplementary Table 8)**. L919X KI mice only showed a
210 trend for acidosis ($p = 0.068$) (**Supplementary Table 7)**, suggesting a more severe
211 phenotype in R607H KI/KI than in L919X KI/KI mice. Notably, in both L919X and R607H

212 KI/KI mutant mice, plasma sodium and chloride concentrations were significantly
213 increased compared to WT littermates and compared to steady state **(Figure 3 A & B, G**
214 **&H, Supplementary Tables 7 & 8**), suggesting a dehydrated state in KI mice. Given the
215 significant hypernatremia and hyperchloremia in both mutant animals, we wondered
216 whether the renin-angiotensin-aldosterone system (RAAS) or dehydration was activated
217 in mutant mice. Indeed, we observed a higher renin mRNA abundance in homozygous
218 R607H KI mice with a similar trend in L919X KI/KI mice (**Figure 3 C, I)**. We next quantified
219 water consumption (**Figure 3 E, K)**, urine osmolality (**Figure 3 D, J**), and plasma
220 hemoglobin and hematocrit levels for both strains (**Supplementary Tables 7 & 8)**. While
221 no difference in urine osmolality was observed compared to WT littermates (**Figure 3 D,**
222 **J)**, homozygous R607H and L919X mice had reduced water consumption (**Figure 3 E,**
223 **K)**, despite increased hemoglobin concentration in homozygous R607H mice
224 (**Supplementary Table 8).** These results suggest an abnormal salt handling or impaired
225 osmosensing with activation of the RAAS and/or potential dehydration in these mice.
226
227 *Salt-depleted acid loading reveals a salt wasting nephropathy in homozygous L919X and*
228 *R607H KI mice.*
229 Similarly to the sodium depletion diet alone, both homozygous L919X and R607H
230 KI mice acidified their urine, although not to the same extent as their WT littermates
231 **(Figure 4 A & 5 A).** R607H KI/KI mice excreted significantly less ammonium compared
232 to WT (**Figure 5 B)**, while L919X KI/KI mice (**Figure 4 B)** showed no difference compared
233 to their controls, although both genotypes increased overall ammonium excretion at day
234 14 compared to day 0 (**Figure 4 B & 5 B).** The salt-depleted acid diet also revealed a
235 pronounced urinary sodium-losing phenotype in homozygous L919X and R607H KI mice
236 (**Figure 4 C&F, Figure 5 C&F**), in agreement with observations from dRTA patients under
237 similar physiological conditions[12]. Distinct phenotypes were observed concerning renal
238 potassium and chloride handling (**Figure 4 & 5 D, E, G, H**). L919X KI/KI mice exhibited
239 urinary chloride loss with no difference in potassium excretion compared to WT mice
240 (**Figure 4 D & E)**. In contrast, R607H KI/KI mice displayed lower urinary potassium and
241 chloride excretion (**Figure 5 D & E)**. These experiments demonstrate that in mice, both
242 the Ae1 L919X and R607H mutation lead to urinary sodium loss and inability to maximally
243 acidify their urine, thus reproducing major features observed in patients suffering with
244 type 1 dRTA.
245
246 *Paracellular proteins claudin 4 and claudin 10b are upregulated in dRTA mutant mice.*

247 Given the alkaline urine and the urinary sodium loss after salt depleted acid
248 loading, we quantified mRNA and protein levels of specific markers of the CD, the thick
249 ascending limb (TAL) and the distal convoluted tubule (DCT) in KI/KI mice and the
250 respective WT littermates (**Figure 6, Supplementary Figures 3 - 4)**.
251 We found increased mRNA and protein levels of the paracellular pores claudin 4
252 and claudin 10b, in both L919X KI/KI and R607H KI/KI mice (**Figure 6 A-H**). Claudin-4 is
253 a paracellular chloride pore and a sodium pore blocker expressed in the thin ascending
254 limb of Henle's loop, the distal tubule and CD[35–37], while claudin 10b is a sodium pore in
255 the TAL[38–40]. These findings suggest a common compensatory mechanism via the
256 paracellular pathway in the loop of Henle of both mutant strains.
257 The salt-depleted acid challenge also revealed a downregulation of A-IC and B-IC
258 marker gene expression in R607H KI/KI mice, with similar trends in L919X KI/KI mice
259 (**Supplementary Figure 3 & 4 A - I**)**.** There was no clear trend for principal cell markers
260 between KI/KI mice and WT littermates. In agreement with decreased numbers of ICs
261 reported for R607H KI/KI mice[31], kAe1 and B1-ATPase mRNA or protein abundances in
262 whole kidney lysate were significantly reduced compared to WT littermates
263 (**Supplementary Figure 3 & 4 A, C, K**)**.** Messengers for pendrin and AE4 were
264 significantly reduced in R607H KI/KI mice, with a similar trend in L919X KI/KI mice
265 (**Supplementary Figure 3 & 4 C, E**). Increased NDCBE mRNA abundance was observed
266 in R607H KI/KI mice with a similar trend in L919X KI/KI mice (**Supplementary Figure 3**
267 **& 4 D**).
268 Given the higher abundance of the TAL-specific claudin-10b in both mutant mouse lines
269 (**Figure 6 C, D, G, H**)**,** we investigated gene expression of various transporters from prior
270 nephron segments (**Supplementary Figure 3 & 4 H – J, M**)**.** The mRNA abundance of
271 the DCT sodium-chloride cotransporter (NCC) was significantly lower in L919X KI/KI mice
272 with a similar trend in R607H KI mice (**Supplementary Figure 3 & 4 J**). We finally
273 assessed the mRNA abundance of the sodium/potassium/chloride cotransporter NKCC2
274 and sodium/proton exchanger NHE3 in whole kidneys, with the caveat that NHE3 is also
275 abundantly expressed in the proximal tubule. These levels did not differ between L919X
276 KI/KI and WT counterparts, but were significantly decreased in R607H KI/KI mice
277 compared to WT littermates (**Supplementary Figure 3 & 4 H, I**). Overall, these results
278 highlight paracellular adaptations in both KI/KI mice, potentially in an attempt to maintain
279 salt homeostasis.
280
281
282

Discussion

In this study, we characterized a second dRTA mouse model that carries the murine Ae1 L919X mutation orthologous to human dominant R901X dRTA mutation. We focused on homozygous mice as they display a stronger phenotype than heterozygotes more representative of dRTA patients' symptoms. In agreement with the previously published R607H KI/KI model, at baseline, the L919X KI/KI mice exhibit an alkaline urine compared to WT littermates, mimicking the main physiological defect observed in dRTA patients. In perfused kidneys from homozygous L919X and R607H KI mice, we observed decreased Ae1 gene expression suggesting a loss of A-ICs. Overall, our results support that both L919X and R607H KI/KI mouse lines reproduce the alkaline urine seen in dRTA and thus are good models to investigate the underlying pathophysiology.

Our results also reveal a more pronounced phenotype in R607H KI/KI compared to L919X KI/KI mice with slight differences in abundance of mRNA of Henle's loop and CD markers. One study reporting dominant dRTA mutations in the *SLC4A1* gene found that despite phenotypic similarities, the R901X mutation caused a milder phenotype than the R598H. This includes a lower plasma bicarbonate concentration and a more severe hypokalemia in patients with the R589H mutation compared to R901X[21]. Our results confirm this trend with significant differences observed in R607H KI/KI mice versus WT littermates but only similar trends in the L919X KI mice.

We challenged homozygous Ae1 L919X and R607H KI/KI mice and the respective controls with an acute salt-depleted diet or a salt-depleted diet in combination with an acid challenge to assess whether these mice develop a sodium wasting phenotype as shown for some dRTA patients[12]. Both dRTA mutant mice exhibit renal sodium loss compared to WT controls. Both KI/KI mice had elevated plasma sodium and chloride levels with increased abundance of renal renin mRNA suggestive of a volume contracted state despite a similar volume of water consumed and urine osmolality. Importantly, we found an increase in claudin 4 and claudin 10b gene and protein expression in both homozygous L919X and R607H KI mice compared to WT. A previous study feeding a salt restricted diet to a B1-H^+-ATPase knockout mouse model elucidated one mechanism: loss of *Atp6v1b1* impaired sodium reabsorption via pendrin/NDCBE in B-ICs. These mice also had increased urinary ATP and prostaglandin E2 (PGE2) release (known sodium movement inhibitors), which decreased ENaC expression on PCs further contributing to sodium wasting[41]. Consistent with these findings, our experiments showed decreased pendrin and Ae4 gene expression levels, while NDCBE gene expression was increased in R607H KI/KI mice. We also observed increased γ-ENaC (SCNN1G) mRNA and protein

319 abundance in R607H KI/KI, but no significant difference in renal outer medullary
320 potassium channel ROMK gene expression. These trends were also observed in L919X
321 KI/KI mice, with the additional finding of decreased NCC mRNA abundance.
322
323 Both mouse lines displayed a similar alteration in their paracellular pathway in
324 Henle's loop as an increase in claudin-4[6,45,4] and claudin-10b[42] mRNA abundance was
325 observed after acid challenge with salt depletion. Claudin-4 functionally interacts with
326 kAe1, as expressing the exchanger in immortalized inner medullary collecting duct cells
327 increases transepithelial permeability to both sodium and chloride in a mechanism
328 dependent in part on claudin-4 and with-no-lysine kinase 4[42,43]. Although present in tight
329 junction, claudin 10b also colocalizes with the sodium/potassium ATPase and chloride
330 channels in the basolateral infoldings of the TAL[39]. While its role there remains unclear,
331 it may play a crucial role in facilitating high electrolyte flow, and preventing basolateral
332 water influx. Therefore, increased expression of claudin 10b may represent a
333 compensatory mechanism to enhance urine concentration and regulate electrolyte
334 balance.
335
336 The upregulation of claudins in Henle's loop points towards a possible
337 compensatory role of this segment in urinary acidification and sodium reabsorption. The
338 ascending limb of Henle's loop is a site for urinary acidification via the combined action
339 of apical NHE3 and basolateral NBCn1[44,45]. As shown by our experiments, mutant mice
340 still acidify their urine although they are kAE1-depleted, which points towards a possible
341 contribution of this segment to urinary acidification, in addition to sodium and chloride
342 reabsorption. The function of acid-base transporters is tightly coupled to that of salts in
343 the TAL, through apical NHE3 and the basolateral electroneutral sodium bicarbonate co-
344 transporter, NBCn1[49, 50]. NBCn1 facilitates urine acidification during metabolic acidosis[50],
345 promoting ammonium reabsorption across the renal tubules, rapidly restoring arterial
346 blood pH and facilitating its secretion by the CD[51]. Previous work reported that R607H
347 KI/KI mice have increased NCBn1 protein abundance at steady state compared to WT
348 mice[33]. The potential upregulation of this protein in the KI/KI mice lines could provide an
349 explanation for their ability to effectively regulate plasma pH and acidify their urine to
350 some extent despite the loss of IC. Additionally, NKCC2 and ROMK in the TAL may cause
351 a net chloride reabsorption creating a lumen-positive transepithelial potential driving
352 paracellular sodium reabsorption through claudin 10b.
353

After the salt-depleted acid challenge, we detected a significantly decreased mRNA abundance of NHE3 and NKCC2 in homozygous R607H KI mice compared to WT. The relevance of this finding may be limited as both NHE3 and NKCC2 proteins are post-translationally regulated. NKCC2 regulation occurs via membrane trafficking, phosphorylation, and protein-protein interactions[46]. NHE3 is regulated through phosphorylation, and its activity can be inhibited by aldosterone[47,48], which may be relevant in the context of salt depletion.

There are some limitations to this work. Although the KI/KI mice reproduced some symptoms of dRTA, they are not exhibiting them all. First, these mice knocked in with a dominant dRTA mutation display a milder phenotype than dRTA patients. Indeed homozygous mice exhibited acidemia only after an acid challenge[31], while heterozygous dRTA patients with dominant mutations have overt acidemia at baseline. We hypothesize that this is due to the difference in diet between rodents and humans. Therefore, we have focused our study on homozygous mice. Second, these mice do not exhibit hypercalciuria, nephrocalcinosis and kidney stones that are commonly observed in dRTA patients. The reason for this discrepancy is unknown. Importantly, mice with a disruption on *Atp6v1b1*, which in humans causes dRTA, also lack the hypercalciuria, nephrocalcinosis and overt acidemia[41] seen in these patients, pointing to some limitations inherent to these mouse models. However, although a limitation, the lack of these symptoms allowed us to investigate other dRTA symptoms without the caveats of kidney stones and nephrocalcinosis.

Overall, our results show that both L919X and R607H and KI/KI mice recapitulate some dRTA symptoms, including the urinary sodium loss seen in patients. Our results reveal physiological mechanisms for this complex disease and point to a potential compensatory acidification and salt reabsorption in earlier nephron segments.

382 **Acknowledgments**

383 This study was funded by the Canadian Institutes of Health Research
384 (PJT#168871) and the Kidney Foundation of Canada (2020KHRG-666615) to E.C.
385 C.A.H. was supported by a grant of the DFG (HU 800/7-2). D.E. is supported by a grant
386 from the French National Research Agency (ANR-14-CE12-0013-01), and by the National
387 Center for Precision Diabetic Medicine – PreciDIAB. (ANR-18-IBHU-0001). P.M. received
388 a Canada Graduate Scholarship-Master's graduate studentship from the Canadian
389 Institutes of Health Research, a University of Alberta Graduate Recruitment Scholarship
390 and a Walter H. Johns Graduate Fellowship from the University of Alberta. A.K.M.S.U.
391 received an NSERC CREATE graduate studentship, G.E. received a Graduate Student
392 Engagement Scholarship, a Faculty of Medicine and Dentistry Delnor Scholarship and a
393 Faculty of Medicine and Dentistry 75th Anniversary award. F. C. was awarded an
394 University of Alberta Graduate Recruitment Scholarship.

395

References

1. Mohebbi, N. & Wagner, C. A. Pathophysiology, diagnosis and treatment of inherited distal renal tubular acidosis. *J. Nephrol.* **31**, 511–522 (2018).
2. Alper, S. L. Familial renal tubular acidosis. *J Nephrol* **23 Suppl 1**, S57-76 (2010).
3. Batlle, D., Ghanekar, H., Jain, S. & Mitra, A. Hereditary distal renal tubular acidosis: new understandings. *Annu Rev Med* **52**, 471–484 (2001).
4. Giglio, S., Montini, G., Trepiccione, F., Gambaro, G. & Emma, F. Distal renal tubular acidosis: a systematic approach from diagnosis to treatment. *Journal of Nephrology* **34**, 2073–2083 (2021).
5. Wagner, C. A. *et al.* The pathophysiology of distal renal tubular acidosis. *Nat. Rev. Nephrol. 2023 196* **19**, 384–400 (2023).
6. Fry, A. C. & Karet, F. E. Inherited renal acidoses. *Physiol.* **22**, 202–211 (2007).
7. Karet, F. E. Inherited distal renal tubular acidosis. *J Am Soc Nephrol* **13**, 2178–2184 (2002).
8. Laing, C. M., Toye, A. M., Capasso, G. & Unwin, R. J. Renal tubular acidosis: developments in our understanding of the molecular basis. *Int J Biochem Cell Biol* **37**, 1151–1161 (2005).
9. Unwin, R. J. & Capasso, G. The renal tubular acidoses. *J R Soc Med* **94**, 221–225 (2001).
10. Aronson, P. S. & Giebisch, G. Effects of pH on potassium: New explanations for old observations. *Journal of the American Society of Nephrology* **22**, 1981–1989 (2011).
11. Alonso-Varela, M., Gil-Peña, H. & Santos, F. Incomplete distal renal tubular

419 acidosis in children. *Acta Paediatr.* **109**, 2243–2250 (2020).

420 12. Sebastian, A., McSherry, E., Morris, R. C. & Morris Jr., R. C. Impaired renal
421 conservation of sodium and chloride during sustained correction of systemic
422 acidosis in patients with type 1, classic renal tubular acidosis. *J Clin Invest* **58**,
423 454–469 (1976).

424 13. Lashhab, R., Ullah, A. K. M. S. & Cordat, E. Renal collecting duct physiology and
425 pathophysiology. *Biochem. Cell Biol.* 1–9 (2018). doi:10.1139/bcb-2018-0192

426 14. Roy, A., Al-bataineh, M. M. & Pastor-Soler, N. M. Collecting duct intercalated cell
427 function and regulation. *Clin. J. Am. Soc. Nephrol.* **10**, 305–24 (2015).

428 15. Saxena, V. *et al.* Kidney intercalated cells are phagocytic and acidify internalized
429 uropathogenic Escherichia coli. *Nat. Commun.* **12**, (2021).

430 16. Purkerson, J. M., Heintz, E. V., Nakamori, A. & Schwartz, G. J. Insights into
431 acidosis-induced regulation of SLC26A4 (pendrin) and SLC4A9 (AE4)
432 transporters using three-dimensional morphometric analysis of β-intercalated
433 cells. *Am. J. Physiol. - Ren. Physiol.* **307**, F601 (2014).

434 17. Peña-Münzenmayer, G., George, A. T., Shull, G. E., Melvin, J. E. & Catalán, M.
435 A. Ae4 (Slc4a9) is an electroneutral monovalent cation-dependent Cl-/HCO3-
436 exchanger. *J. Gen. Physiol.* **147**, 423–436 (2016).

437 18. Wall, S. M., Verlander, X. J. W. & Romero, C. A. The renal physiology of pendrin-
438 positive intercalated cells. *Physiological Reviews* **100**, 1119–1147 (2020).

439 19. Bruce, L. J. *et al.* Familial distal renal tubular acidosis is associated with mutations
440 in the red cell anion exchanger (Band 3, AE1) gene. *J Clin Invest* **100**, 1693–1707
441 (1997).

442 20. Bruce, L. J. *et al.* Band 3 mutations, renal tubular acidosis and South-East Asian
443 ovalocytosis in Malaysia and Papua New Guinea: loss of up to 95% band 3
444 transport in red cells. *Biochem J* **350 Pt 1**, 41–51 (2000).
445 21. Karet, F. E. *et al.* Mutations in the chloride-bicarbonate exchanger gene AE1
446 cause autosomal dominant but not autosomal recessive distal renal tubular
447 acidosis. *Proc Natl Acad Sci U S A* **95**, 6337–6342 (1998).
448 22. Jarolim, P. *et al.* Autosomal dominant distal renal tubular acidosis is associated in
449 three families with heterozygosity for the R589H mutation in the AE1 (Band 3) Cl-
450 /HCO3/- exchanger. *J. Biol. Chem.* **273**, 6380–6388 (1998).
451 23. Arakawa, T. *et al.* Crystal structure of the anion exchanger domain of human
452 erythrocyte band 3. *Science (80-.).* **350**, 680–684 (2015).
453 24. Zhekova, H. R. *et al.* CryoEM structures of anion exchanger 1 capture multiple
454 states of inward- and outward-facing conformations. *Commun. Biol.* **5**, 1–13
455 (2022).
456 25. Reithmeier, R. A. F. *et al.* Band 3, the human red cell chloride/bicarbonate anion
457 exchanger (AE1, SLC4A1), in a structural context. *Biochimica et Biophysica Acta*
458 *- Biomembranes* **1858**, 1507–1532 (2016).
459 26. Cordat, E. *et al.* Dominant and recessive distal renal tubular acidosis mutations of
460 kidney anion exchanger 1 induce distinct trafficking defects in MDCK cells. *Traffic*
461 **7**, 117–128 (2006).
462 27. Toye, A. M., Banting, G. & Tanner, M. J. A. Regions of human kidney anion
463 exchanger 1 (kAE1) required for basolateral targeting of kAE1 in polarized kidney
464 cells: Mis-targeting explains dominant renal tubular acidosis (dRTA). *J. Cell Sci.*

465 **117**, 1399–1410 (2004).

466 28. Quilty, J. A. A., Cordat, E. & Reithmeier, R. A. F. A. Impaired trafficking of human
467 kidney anion exchanger (kAE1) caused by hetero-oligomer formation with a
468 truncated mutant associated with distal renal tubular acidosis. *Biochem J* **368**,
469 895–903 (2002).

470 29. Toye, A. M., Bruce, L. J., Unwin, R. J., Wrong, O. & Tanner, M. J. Band 3 Walton,
471 a C-terminal deletion associated with distal renal tubular acidosis, is expressed in
472 the red cell membrane but retained internally in kidney cells. *Blood* **99**, 342–7.
473 (2002).

474 30. Cordat, E., Li, J. & Reithmeier, R. A. F. Carboxyl-terminal truncations of human
475 anion exchanger impair its trafficking to the plasma membrane. *Traffic* **4**, 642–651
476 (2003).

477 31. Mumtaz, R. *et al.* Intercalated Cell Depletion and Vacuolar H+-ATPase
478 Mistargeting in an Ae1 R607H Knockin Model. *J. Am. Soc. Nephrol.* **28**, 1507–
479 1520 (2017).

480 32. Stehberger, P. A. *et al.* Distal renal tubular acidosis in mice lacking the AE1
481 (band3) Cl-/HCO3- exchanger (slc4a1). *J Am Soc Nephrol* **18**, 1408–1418 (2007).

482 33. DeFranco, P. E., Haragism, L., Schmitz, P. G., Bastani, B. & Li, J. P. Absence of
483 vacuolar H+-ATPase pump in the collecting duct of a patient with hypokalemic
484 distal renal tubular acidosis and Sjogren's syndrome. *J. Am. Soc. Nephrol.* **6**,
485 295–301 (1995).

486 34. Vichot, A. A. *et al.* Loss of kAE1 expression in collecting ducts of end-stage
487 kidneys from a family with SLC4A1 G609R-associated distal renal tubular

488 acidosis. *Clin. Kidney J.* **10**, 135–140 (2017).
489 35. Chambrey, R. & Trepiccione, F. Relative Roles of Principal and Intercalated Cells
490 in the Regulation of Sodium Balance and Blood Pressure. *Current Hypertension*
491 *Reports* **17**, (2015).
492 36. Hou, J., Rajagopal, M. & Yu, A. S. Claudins and the kidney. *Annu Rev Physiol* **75**,
493 479–501 (2013).
494 37. Leiz, J. & Schmidt-Ott, K. M. Claudins in the renal collecting duct. *International*
495 *Journal of Molecular Sciences* **21**, (2020).
496 38. Yu, A. S. L. Claudins and the Kidney. *J. Am. Soc. Nephrol.* **26**, 11–19 (2015).
497 39. Quintanova, C. *et al.* Unrecognized role of claudin-10b in basolateral membrane
498 infoldings of the thick ascending limb. *Ann. N. Y. Acad. Sci.* **1517**, 266–278
499 (2022).
500 40. Hou, J., Renigunta, A., Yang, J. & Waldegger, S. Claudin-4 forms paracellular
501 chloride channel in the kidney and requires claudin-8 for tight junction localization.
502 *Proc. Natl. Acad. Sci.* **107**, 18010–18015 (2010).
503 41. Gueutin, V. *et al.* Renal beta-intercalated cells maintain body fluid and electrolyte
504 balance. *J Clin Invest* **123**, 4219–4231 (2013).
505 42. Lashhab, R., Essuman, G., Chavez-Canales, M., Alexander, R. T. & Cordat, E.
506 Expression of the kidney anion exchanger 1 affects WNK4 and SPAK
507 phosphorylation and results in claudin-4 phosphorylation. *Heliyon* **9**, (2023).
508 43. Lashhab, R. *et al.* The kidney anion exchanger 1 affects tight junction properties
509 via claudin-4. *Sci. Rep.* **9**, 3099 (2019).
510 44. de Bruijn, P. I. A. *et al.* Furosemide-induced urinary acidification is caused by

511 pronounced H+ secretion in the thick ascending limb. *Am. J. Physiol. Renal*
512 *Physiol.* **309**, F146–F153 (2015).
513 45. Olsen, J. S. M. *et al.* NBCn1 Increases NH4 + Reabsorption Across Thick
514 Ascending Limbs, the Capacity for Urinary NH4 + Excretion, and Early Recovery
515 from Metabolic Acidosis. *J. Am. Soc. Nephrol.* **32**, 852–865 (2021).
516 46. Ares, G. R., Caceres, P. S. & Ortiz, P. A. Molecular regulation of NKCC2 in the
517 thick ascending limb. *American Journal of Physiology - Renal Physiology* **301**,
518 F1143 (2011).
519 47. Girardi, A. C. C. & di Sole, F. Deciphering the mechanisms of the Na+/H+
520 exchanger-3 regulation in organ dysfunction. *American Journal of Physiology -*
521 *Cell Physiology* **302**, 1569–1587 (2012).
522 48. Watts, B. A., George, T. & Good, D. W. Aldosterone inhibits apical NHE3 and
523 HCO_3^- absorption via a nongenomic ERK-dependent pathway in medullary thick
524 ascending limb. *Am. J. Physiol. Physiol.* **291**, F1005–F1013 (2006).
525
526

527 **Figure Legends**

528 **Figure 1**: Generation and characterization of the L919X KI mice. (**A**)Targeting and
529 screening strategy with murine Ae1 locus (top) and targeted locus (middle) with locus
530 after removal of the selection cassette by Cre recombination. Right, Southern blot result
531 and sequencing validating the introduction of the mutation to the locus. (**B**) Graph
532 representing the gene expression of Ae1 in perfused whole kidney from WT or L919X
533 KI/KI mice. (C) immunofluorescence images from confocal microscopy of WT,
534 heterozygous or homozygous L919X KI/KI mice medullary or cortical kidney sections
535 stained with anti-pendrin (red) or anti-AE1 (green) antibodies. Scale bar corresponds to
536 50 µm. (D) Quantification of A-IC (Ae1 positive) and B-IC (pendrin positive) in the cortex
537 and medulla of WT or homozygous Ae1 L919X KI mice. Error bars correspond to means
538 ± SEM, n = 4-6 kidney sections, ***P < 0.001 using Two-way ANOVA.

539

540 **Figure 2**: At baseline, both R607H and L919X KI/KI mice exhibit an alkaline urine and
541 decreased urinary ammonium secretion. Urinary pH (**A**), ammonium (**B**), osmolality (**C**),
542 sodium/creatinine ratio (**C**), chloride/creatinine ratio (**D**) and potassium/creatinine ratio (**E**)
543 comparison between WT or L919X KI/KI mice. Urinary pH (**G**), ammonium (**H**), osmolality
544 (**I**), sodium/creatinine ratio (**J)**, chloride/creatinine ratio (**K**) and potassium/creatinine ratio
545 (**L**) comparison between WT or R607H KI/KI mice. Error bars correspond to means ±
546 SEM, **P < 0.01, ****P < 0.0001 using Student's t-test or Mann-Whitney test.

547

548 **Figure 3**: After a salt-depleted acid diet, both R607H and L919X KI/KI mice are
549 hypernatremic and hyperchloremic. Plasma sodium (**A**) and chloride (**B**) concentrations

550 from L919X KI/KI mice or WT littermates. (**C**) Renin gene expression in L919X KI/KI mice
551 or WT littermates. Urine osmolality (**D**) and water consumed (**E)** by L919X KI/KI mice or
552 WT littermates over the 14 day-time course of the diet. Plasma sodium (**G**) and chloride
553 (**H**) concentrations from R607H KI/KI mice or WT littermates. (**I**) Renin gene expression
554 in R607H KI/KI mice or WT littermates. Urine osmolality (**J**) and water consumed (**K)** by
555 R607H KI/KI mice or WT littermates over the 14 day-time course of the diet. Error bars
556 correspond to means ± SEM, *P < 0.05, ***P < 0.001, ****P < 0.0001 using Student's t-
557 test or two-way ANOVA with Tukey's multiple comparison test.
558
559 **Figure 4**: After a salt-depleted acid diet, L919X KI/KI mice produce an alkaline urine and
560 waste urinary sodium and chloride. (**A**) Day 14 (left) and trend (right) over the 14
561 experimental days urine pH in L919X KI/KI mice or WT littermates. (**B**) Day 14 (left) and
562 trend (right) urinary ammonium/creatinine ratio in L919X KI/KI mice or WT littermates.
563 Day 14 urinary sodium/creatinine ratio (**C**), sodium/chloride ratio (**D**) and
564 potassium/creatinine ratio (**E**). (**F-H**) trend of sodium/creatinine, sodium/chloride and
565 potassium/creatinine ratios over the time course of the experiment in L919X KI/KI mice
566 or WT littermates. Error bars correspond to means ± SEM, *P < 0.05, **P < 0.01, ***P <
567 0.001, ****P < 0.0001 using Student's t-test or two-way ANOVA with Tukey's multiple
568 comparison test. Note that in panel F, no significant difference between WT and KI mice
569 at Day 14 was detected likely due to the two-way ANOVA statistical test comparing
570 multiple conditions and resulting in a high type I error and p value, but a significant
571 difference was found using a Student's t-test (Figure 3 A).
572

573 **Figure 5**: After a salt-depleted acid diet, R607H KI/KI mice produce an alkaline urine and
574 waste urinary sodium and chloride. (**A**) Day 14 (left) and trend (right) over the 14
575 experimental days urine pH in R607H KI/KI mice or WT littermates. (**B**) Day 14 (left) and
576 trend (right) urinary ammonium/creatinine ratio in R607H KI/KI mice or WT littermates.
577 Day 14 urinary sodium/creatinine ratio (**C**), sodium/chloride ratio (**D**) and
578 potassium/creatinine ratio (**E**). (**F-H**) trend of sodium/creatinine, sodium/chloride and
579 potassium/creatinine ratios over the time course of the experiment in R607H KI/KI mice
580 or WT littermates. Error bars correspond to means ± SEM, *P < 0.05, **P < 0.01, ***P <
581 0.001, ****P < 0.0001 using Student's t-test or two-way ANOVA with Tukey's multiple
582 comparison test. Note that in panel F, no significant difference between WT and KI mice
583 at Day 14 was detected likely due to the two-way ANOVA statistical test comparing
584 multiple conditions and resulting in a high type I error and p value, but a significant
585 difference was found using a Student's t-test (Figure 3 G).
586
587 **Figure 6**: Claudin-4 and claudin-10b are upregulated in both L919X and R607H KI/KI
588 mice after a salt depleted acid diet. Claudin-4 gene expression (**A** & **E**) and protein
589 abundance (**B** & **F**) with a representative immunoblot image (right). Claudin-10b gene
590 expression (**C** & **G**) and claudin-10 protein abundance (**D** & **H**) with a representative
591 immunoblot image (right). Error bars correspond to means ± SEM, *P < 0.05, **P < 0.01,
592 using Student's t-test or two-way ANOVA with Tukey's multiple comparison test.
593
594

595 **Supplementary Table 1**: Primers and Probes Used for qPCR on Mouse Genes

Name	Forward	Reverse	Probe
AE4 NM_N172830	5'-CTCTGTGTCTTTGAGCTTTGC-3'	5'-TCTGCCTATGGTTGCTTCTG-3'	5'-/56-FAM/TGTTTCCTC/ZEN/CTGTGCCTGGGTATTG/3IABKFQ/-3'
alpha-ENaC NM_011324.2	5'-CAGTGATGTCCCTGTCAAGAA-3'	5'-CTTGGGCTTAGGGTAGAAGATG-3'	5'- /56-FAM/TGA TCA AGA /ZEN/AGT GTGGCT GTG CCT /3IABKFQ/ -3'
Atp6v1b1 NM_134157.1	5'-CTTCTCACACTGGTAGGCAAG-	5'-AGTCAGATTTCGAGCAGAATGG-3'	5'-/56-FAM/CCGCTCAAT/ZEN/CGTAGGGTCATTGGC/3IABkFQ/-3'
Cldn10b NM_N021386.1	5'-GCAGCGATCATTAGTCCTCTAC-3'	5'-CCACAGCCACTTATTTTGCC-3'	5-/56-FAM/A ATCGGTAA/ZEN/CGCAGATCTCCACAGG/3IABkFQ/-3'
Cld4 NM_N009903.1	5-'CAGGACTGCCAAGGAGATTC-3'	5-'AACACTTTCTCAGCCCTCTG-3'	5-'/56-FAM/CATAGACGC/ZEN/CATCGCTCAGCCTC/3IABkFQ/-3*
gamma-ENaC NM_N011326.1	5'-GTCAGAGGTGTCATTTGAGCA-3'	5'-GAGAACGAGAAGGGAAAGGC-3'	5'-/56-FAM/TCGGAAGCG/ZEN/GAAAATCAGGGGAA/3IABKFQ/-3'
kAE1 NM_009902.4	5'-AAGAGGTCAAGGAACAGCG-3'	5'-GTACAGGAAGATGCCGAAGAG-3'	5-/56-FAM/CCCACAAGC/ZEN/ACAGAGACCAGGAG/3IABkFQ/-3'
NCC NM_019415	5'-CAGATCAACAGGATGGACGAAG-3'	5'-GCAATCATGTCCTCAAACCG-3'	5'-/56-FAM/TCCCGACAT/ZEN/CAACCAGA AGCCC/3IABkFQ/-3'
NDCBE NM_021530.2	5'-ATGGGAAGATGGTGAGGAAC-3'	5'-ACGTGCTCTTTTGGTCCTG-3'	5'-/56-FAM/AAGGTGCTG/ZEN/GAGACGATGAAGGG/3IABKFQ/-3'
NHE3 NM_N001081060.1	5'-CCAAACAGCAAGAAATCCAGG-3'	5'-TCCCTCTATGGTGTCTTCCTC-3'	5'-/56-FAM/CCAATTTC/ZEN/AGTTCACCCATCA AGCCAC/3IABKFQ/-3'
NKCC2 NM_183354	5'-CAAGGAACATTACCAAGCC-3'	5'-CACCAGTTTGATTGAACTCC-3*	5'-/56-FAM/CAAGAAAGA/ZEN/CGGCAACATCAGCAGC/3IABKFQ/-3'
Pendrin NM_011867	5'-TGATGGAGGCAGAGATGAATG-3'	5'-CAGAAAACACTGAGAGACTG-3'	5-/56-FAM/ATGTTCAGG/ZEN/ATGAGGCCATGCGTAG/3IABkFQ/-3'
Renin	TaqMan Gene Expression Assay (Applied Biosystems) REF# 4331182		

RPLP0 Mm.PT.58.43894205	5'-TTATA ACCCTGA AGGCTCGAC-3'	5'-CGCTTGTACCCATTG ATGATG-3'	5'-/56-FAM/AGGCCCTGC/ZEN/ACTC TCGCTT/3IABkFQ/-3'

596

597

598

599 **Supplementary Table 2**: Antibodies Used for Immunoblotting

Name	Reference	Reference	Dilution
Rb anti-Claudin-10	Primary	Antibodies.com	1:1000
Rb anti-Claudin-4	Primary	Invitrogen	1:1000
Rb anti-ENaC gamma	Primary	StressMarq Biosciences Inc	1:5000
Direct-Blot HRP anti-β Actin	Primary	BioLegend	1:10000

600
601

602
603
604 **Supplementary Table 3.** Baseline Plasma Characterization of WT and L919X Ae1 KI/KI Mice.
605

Parameter	Units	WT (n=10)	L919X AE1 KI/KI (=10)	p-value
Na^+	mM	147.5 ± 0.563	146.9 ± 0.623	0.4327
Cl^-	mM	118.8 ± 0.964	119.6 ± 1.536	0.6644
K^+	mM	4.633 ± 0.167	4.610 ± 0.196	0.7029
HCO_3^-	mM	18.38 ± 0.563	19.95 ± 0.511	0.0930
pH		7.289 ± 0.002	7.249 ± 0.009	0.1186
TCO_2	mmHg	19.50 ± 0.749	21.30 ± 0.517	0.0636
BUN	mg/dl	22.70 ± 1.382	19.80 ± 0.987	0.1050
Glucose	mg/dl	181 ± 13.11	198.3 ±10.58	0.3181
HCT	%	36.80 ± 0.554	36 ± 0.789	0.4174
pCO2	mmHg	38.99 ± 2.856	45.75 ± 1.595	0.0525
AnGAP	mM	14.6 ± 0.618	13.22 ± 1.325	0.1197
Hb	g/dl	12.53 ± 0.188	12.23 ± 0.269	0.3729
BEecf	mM	-8.100 ±0.781	-7.100 ± 0.504	0.2963

606 *Data is presented as mean ± SEM. Student's T-Test or Mann-Whitney test used where*
607 *appropriate.*

608
609 **Supplementary Table 4.** Baseline Plasma Characterization of WT and R607H Ae1 KI/KI Mice.
610

Parameter	Units	WT (n=11)	R607H AE1 KI/KI (n=9)	p-value
Na^+	mM	146.4 ± 0.472	147.1 ± 0.586	0.3148
Cl^-	mM	118.2 ±1.110	118.5 ± 0.619	0.1409
K^+	**mM**	**4.5 ± 0.142**	**4.920 ± 0.077***	**0.0207**
HCO_3^-	mM	18.66 ±0.627	19.07 ±0.463	0.6142
pH		7.256 ± 0.014	7.258 ± 0.013	0.9102
TCO_2	mmHg	19.91 ± 0.653	20.20 ± 0.533	0.7370
BUN	**mg/dl**	**21.09 ± 1.351**	**23.60 ± 0.921***	**0.0438**
Glucose	mg/dl	196.3 ± 7.065	197.3 ± 12.31	0.9417
HCT	%	37.73 ± 1.221	38.60 ± 0.340	0.5178
pCO2	mmHg	42.05 ± 1.467	42.72 ± 1.410	0.7417
AnGAP	mM	13.27 ± 1.538	14.60 ± 0.600	0.9863
Hb	g/dl	12.82 ± 0.414	13.14 ± 0.117	0.4826
BEecf	mM	-8.545 ± 0.731	-8.100 ± 0.586	0.5666

611 *Data is presented as mean ± SEM. Student's T-Test or Mann-Whitney test used where*
612 *appropriate.* ***Significant data is bolded.***
613
614

615
616 **Supplementary Table 5.** Plasma Characterization of WT and L919X Ae1 KI/KI Mice Following
617 24 hours of Salt Restriction
618

Parameter	Units	WT (n=10)	L919X AE1 KI/KI (n=10)	p-value
Na^+	mM	147.9 ± 0.690	147.7 ± 0.578	0.8268
Cl^-	mM	117.6 ± 0.897	120.9 ± 1.329	0.0543
K^+	mM	4.980 ± 0.158	5.180 ± 0.464	0.5661
HCO_3^-	mM	20.59 ± 0.613	20.40 ± 0.825	0.8554
pH		7.240 ± 0.021	7.248 ± 0.033	0.8469
TCO_2	mmHg	22.20 ± 0.593	21.80 ± 0.854	0.7048
BUN	mg/dl	30.10 ± 4.365	23.30 ± 0.989	0.1249
Glucose	mg/dl	164.5 ± 12.69	157.1 ± 9.719	0.6490
HCT	%	40.70 ± 0.667	38.90 ± 0.690	0.1152
pCO2	mmHg	47.95 ± 1.127	47.74 ± 3.411	0.9540
AnGAP	mM	14.90 ± 0.795	11.89 ± 1.369	0.0677
Hb	g/dl	13.84 ± 0.225	13.22 ± 0.237	0.0741
BEecf	mM	-6.900 ± 0.971	-6.800 ± 1.073	0.9457

619 *Data is presented as mean ± SEM. Student's T-Test or Mann-Whitney test used where*
620 *appropriate.* ***Significant data is bolded.***
621
622

623
624 **Supplementary Table 6.** Plasma Characterization of WT and R607H Ae1 KI/KI Mice Following
625 24 hours of Salt Restriction
626

Parameter	Units	WT (n=12)	R607H AE1 KI/KI (n=14)	p-value
Na^+	mM	146.3 ± 0.890	148.1 ± 0.275	0.8166
Cl^-	mM	121.5 ± 2.062	122.9 ± 0.769	0.5196
K^+	**mM**	**4.475 ± 0.100**	**4.843 ± 0.100**	**0.0162**
HCO_3^-	mM	19.04 ± 0.965	18.39 ± 0.540	0.5437
pH		7.203 ± 0.021	7.215 ± 0.014	0.6389
TCO_2	mmHg	20.50 ± 1.004	19.86 ± 0.592	0.9305
BUN	mg/dl	23.75 ± 1.473	25.00 ± 1.267	0.5236
Glucose	mg/dl	154.5 ± 11.59	182.6 ± 9.245	0.0667
HCT	%	37.50 ± 2.183	37.86 ± 0.710	0.1096
pCO2	mmHg	48.33 ± 2.356	45.75 ± 1.901	0.3983
AnGAP	mM	10.25 ± 2.394	11.64 ± 0.608	0.1453
Hb	g/dl	12.76 ± 0.741	12.86 ± 0.246	0.0994
BEecf	mM	-9.000 ± 1.206	-9.357 ± 0.608	0.7847

627 *Data is presented as mean ± SEM. Student's T-Test or Mann-Whitney test used where*
628 *appropriate.* ***Significant data is bolded.***
629
630

631
632 **Supplementary Table 7.** Plasma Characterization of WT and L919X Ae1 KI/KI Mice Following
633 Salt Depleted Acid Load.
634

Parameter	Units	WT (n=14)	L919X AE1 KI/KI (n=14)	p-value
Na^+	**mM**	**149.4 ± 0.644**	**156.4 ± 1.152**	**< 0.0001**
Cl^-	**mM**	**126.9 ± 2.087**	**135.1 ± 0.900**	**0.0140**
K^+	mM	4.777 ± 0.154	4.669 ± 0.170	0.6430
HCO_3^-	mM	15.63 ± 0.940	13.88 ± 0.470	0.1164
pH		7.170 ± 0.030	7.131 ± 0.014	0.0683
TCO_2	**mmHg**	**17.62 ± 0.789**	**15.15 ± 0.504**	**0.0147**
BUN	**mg/dl**	**23.75 ± 0.954**	**33.62 ± 1.723**	**< 0.0001**
Glucose	mg/dl	148.9 ± 12.93	131.92 ± 5.054	0.2452
HCT	%	37.38 ± 1.274	37.46 ± 1.264	0.9713
pCO2	mmHg	42.84 ± 2.581	41.72 ± 1.632	0.7216
AnGAP	mM	13.33 ± 1.694	13.09 ± 0.948	0.9042
Hb	g/dl	12.70 ± 0.432	12.74 ± 0.430	0.9713
BEecf	mM	-12.93 ± 1.294	-15.31 ± 0.603	0.1169

635 *Data is presented as mean ± SEM. Student's T-Test or Mann-Whitney test used where*
636 *appropriate.* ***Significant data is bolded.***
637
638

639
640 **Supplementary Table 8.** Plasma Characterization of WT and R607H Ae1 KI/KI Mice Following
641 Salt Depleted Acid Load.
642

Parameter	Units	WT (n=14)	R607H AE1 KI/KI (n = 18)	p-value
Na^+	**mM**	**145.2 ± 0.882**	**156.4 ± 0.903**	**< 0.0001**
Cl^-	**mM**	**126.8 ± 1.959**	**138.6 ± 0.536**	**< 0.0001**
K^+	mM	4.557 ± 0.229	4.406 ± 0.185	0.6069
HCO_3^-	**mM**	**14.15 ± 0.921**	**11.64 ± 0.775**	**0.0448**
pH		**7.192 ± 0.025**	**7.085 ± 0.020**	**0.0016**
TCO_2	mmHg	15.29 ± 0.963	12.83 ± 0.797	0.0572
BUN	**mg/dl**	**22.50 ± 1.725**	**34.17 ± 3.618**	**0.0026**
Glucose	**mg/dl**	**163.2 ± 11.93**	**118.8 ± 7.284**	**0.0024**
HCT	%	34.00 ± 2.176	32.56 ± 2.297	0.8434
pCO2	mmHg	46.21 ± 1.429	38.56 ± 2.400	0.4397
AnGAP	mM	10.08 ± 2.065	13.43 ± 1.462	0.6004
Hb	**g/dl**	**11.56 ± 0.739**	**13.55 ± 0.189**	**0.0489**
BEecf	**mM**	**-14.07 ± 1.273**	**-18.22 ± 0.967**	**0.0129**

643 *Data is presented as mean ± SEM. Student's T-Test or Mann-Whitney test used where*
644 *appropriate.* ***Significant data is bolded.***
645

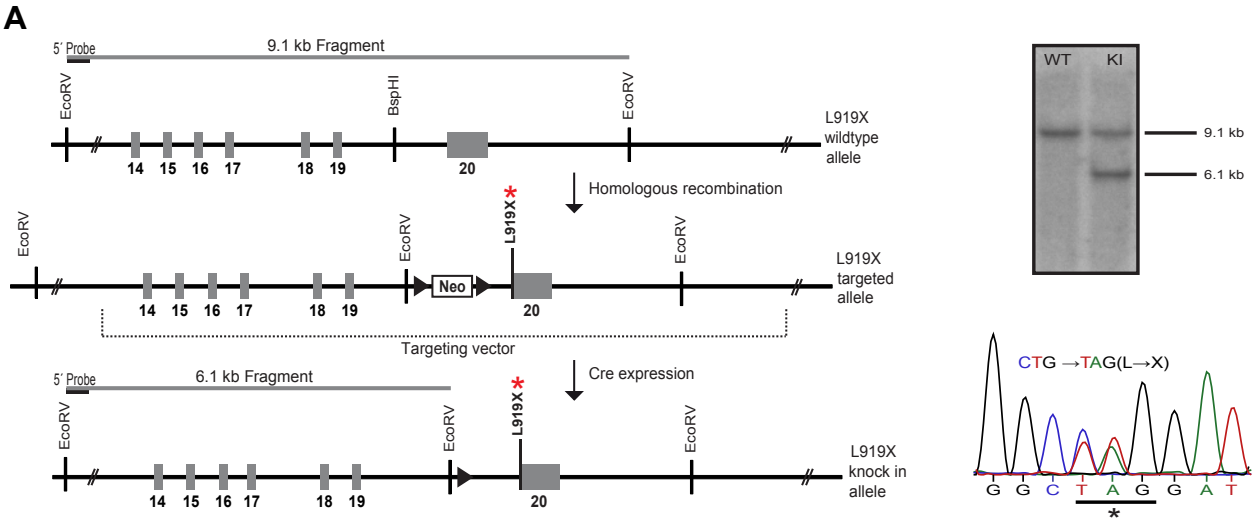

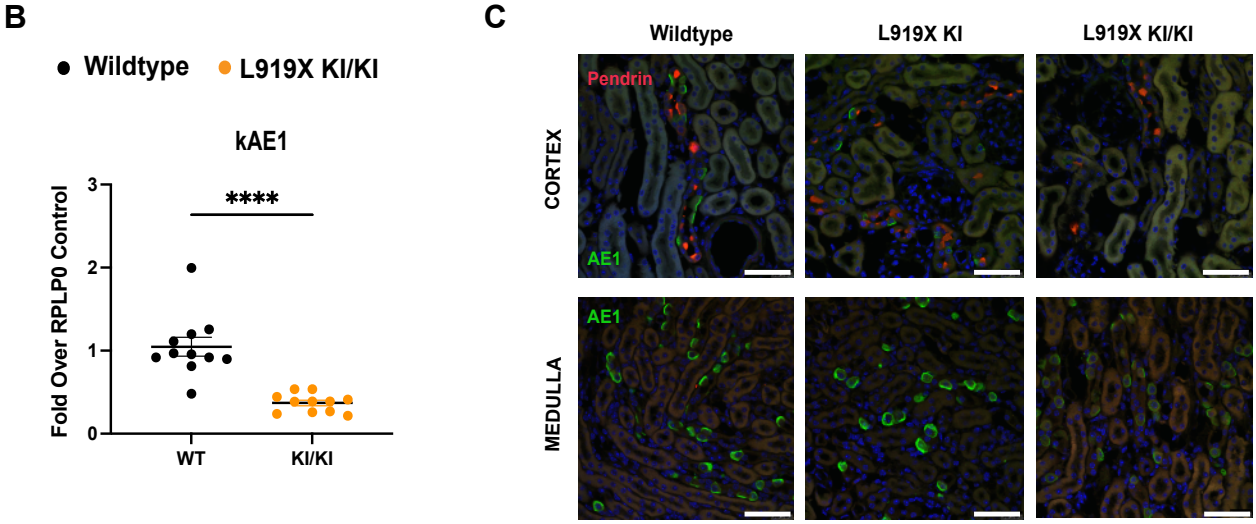

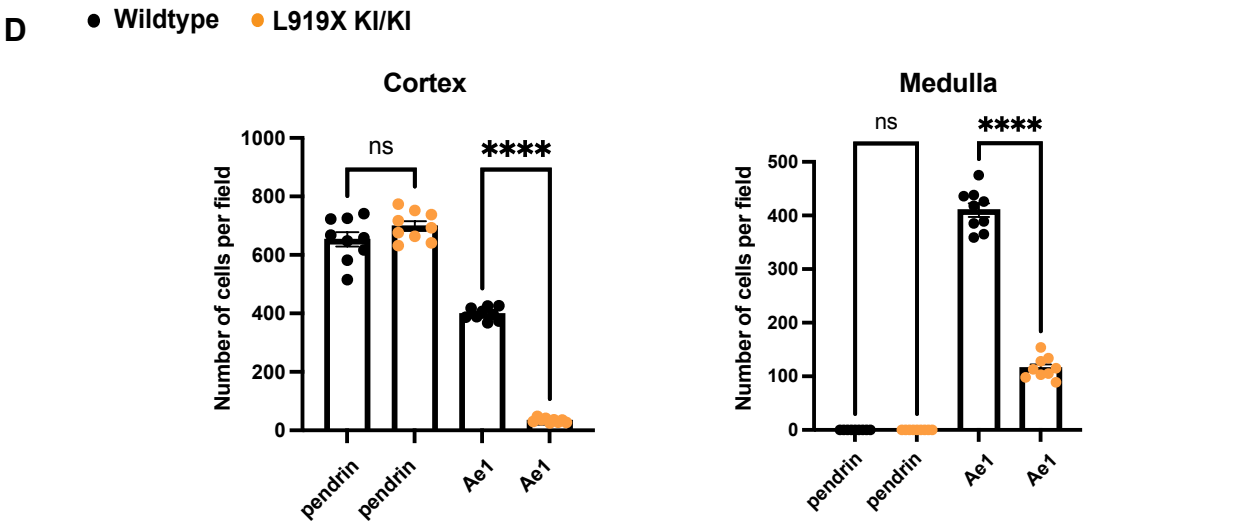

Figure 1 Mungara et al.

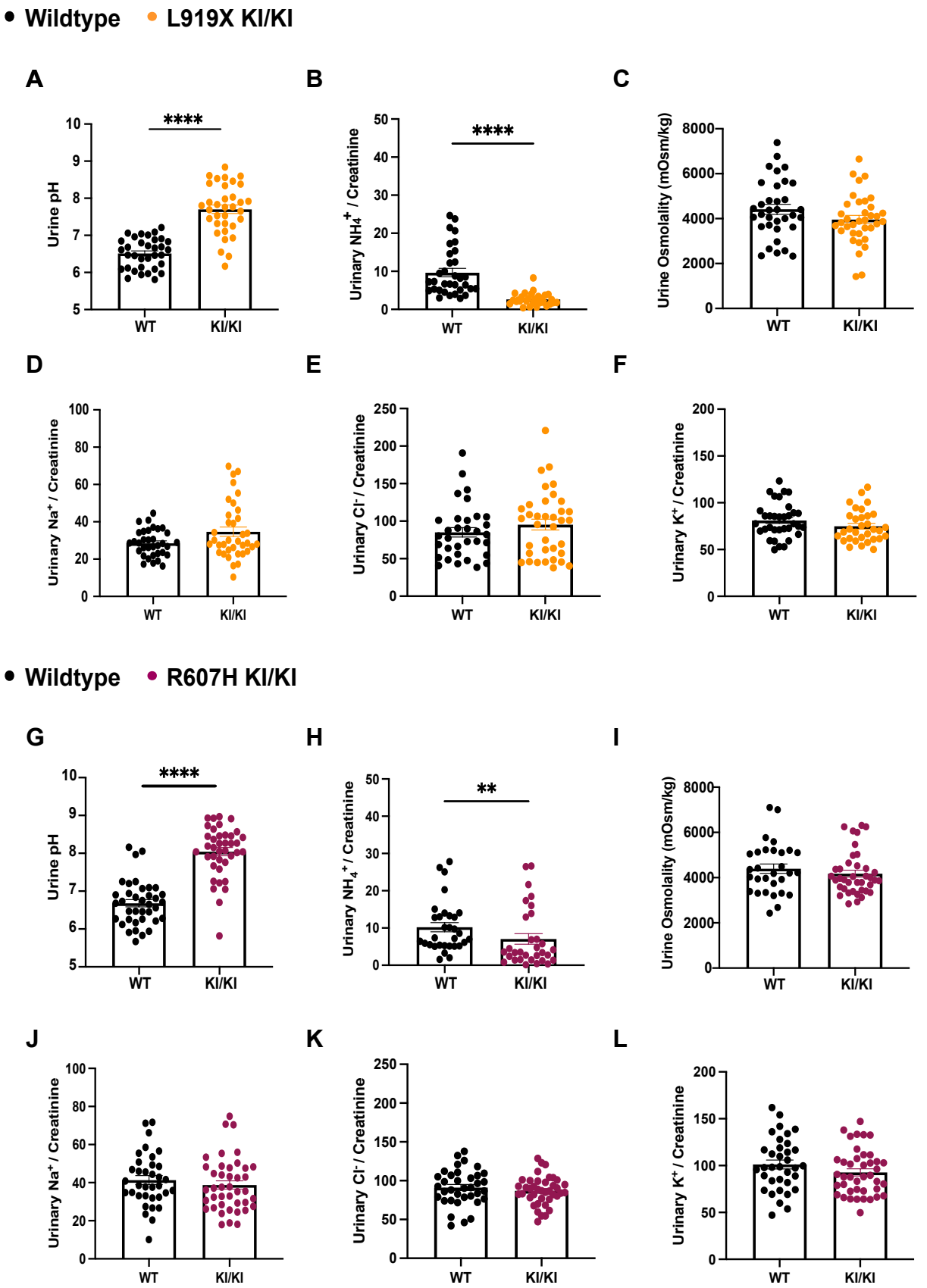

Figure 2 Mungara et al.

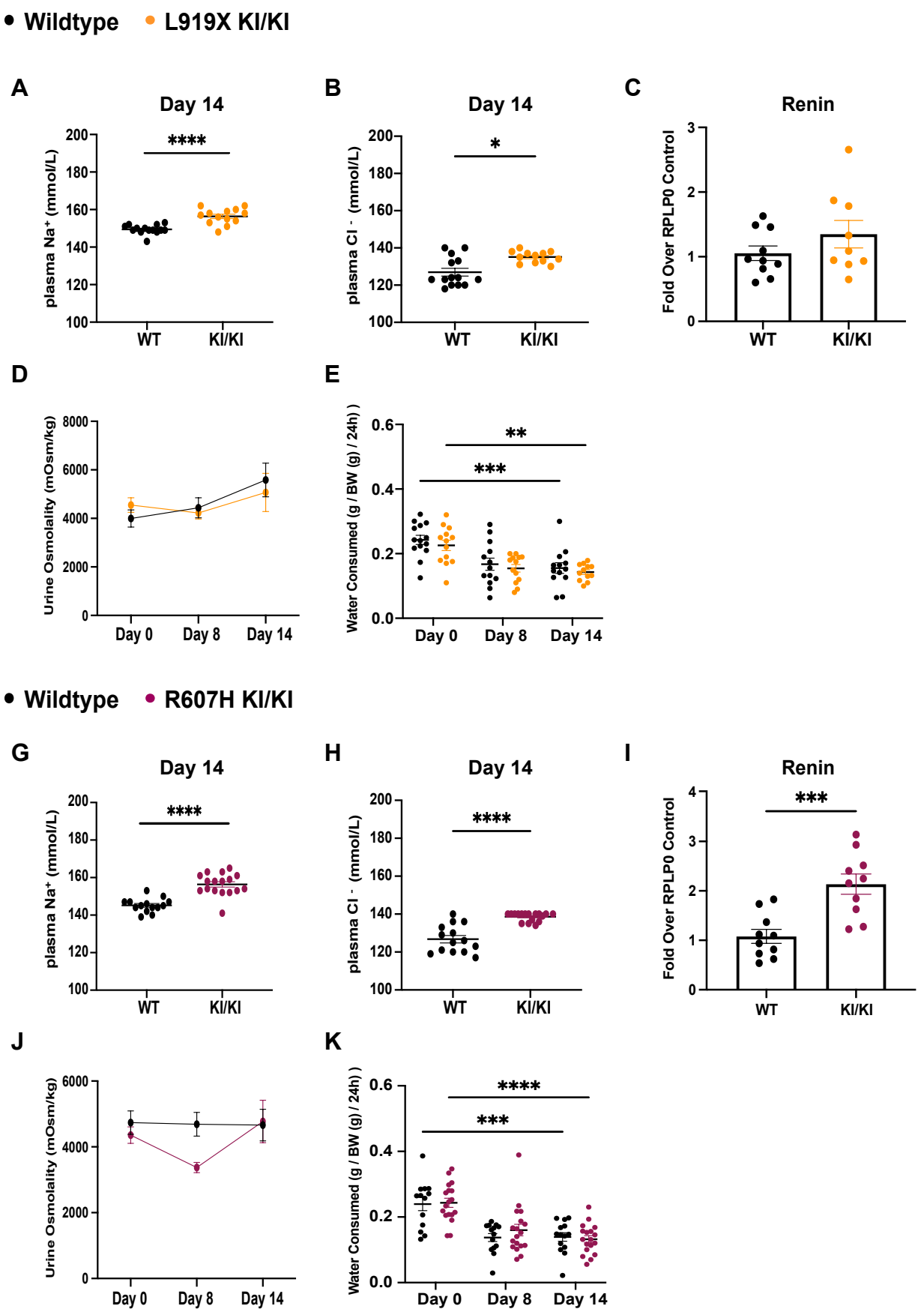

Figure 3 Mungara et al.

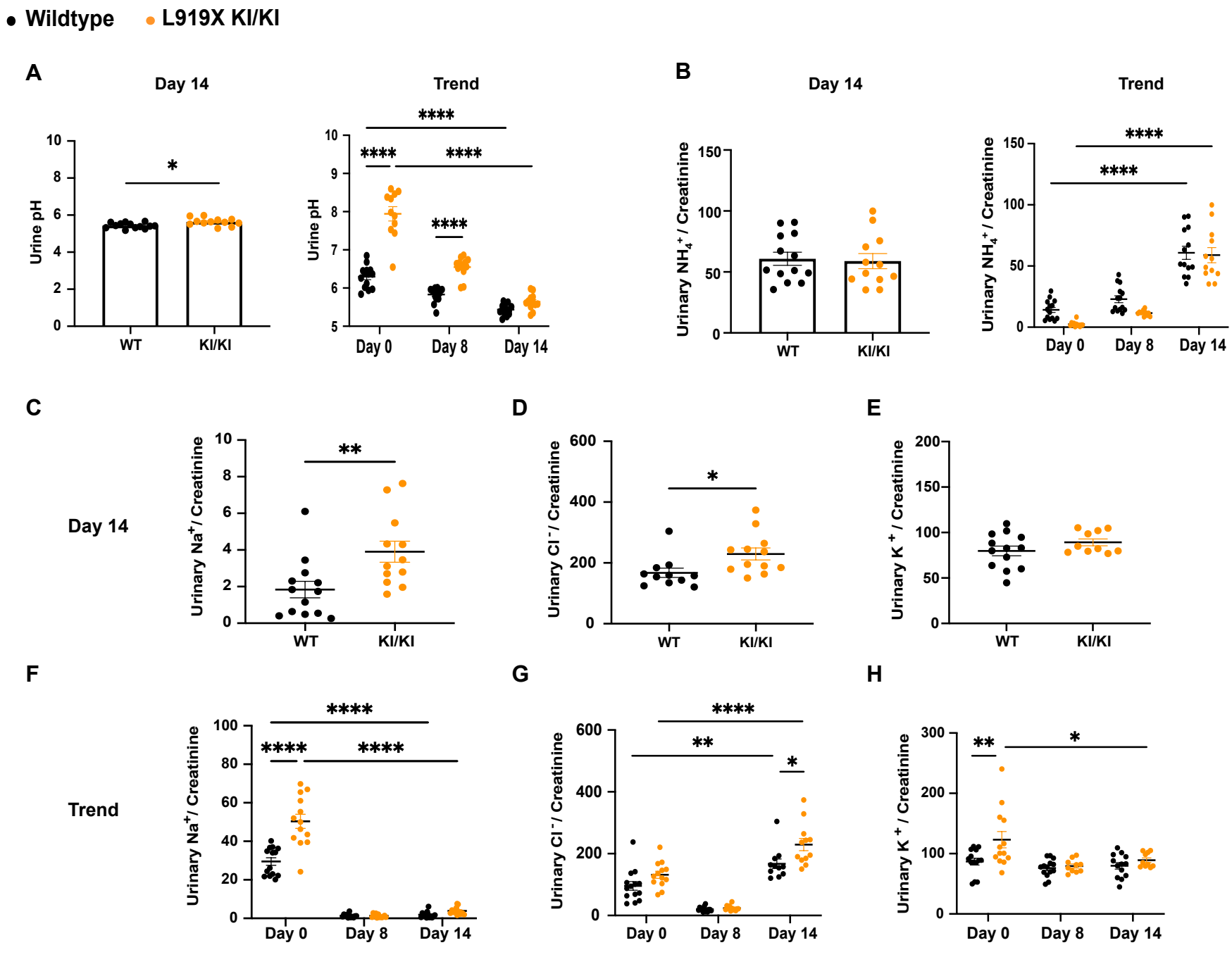

Figure 4 Mungara et al.

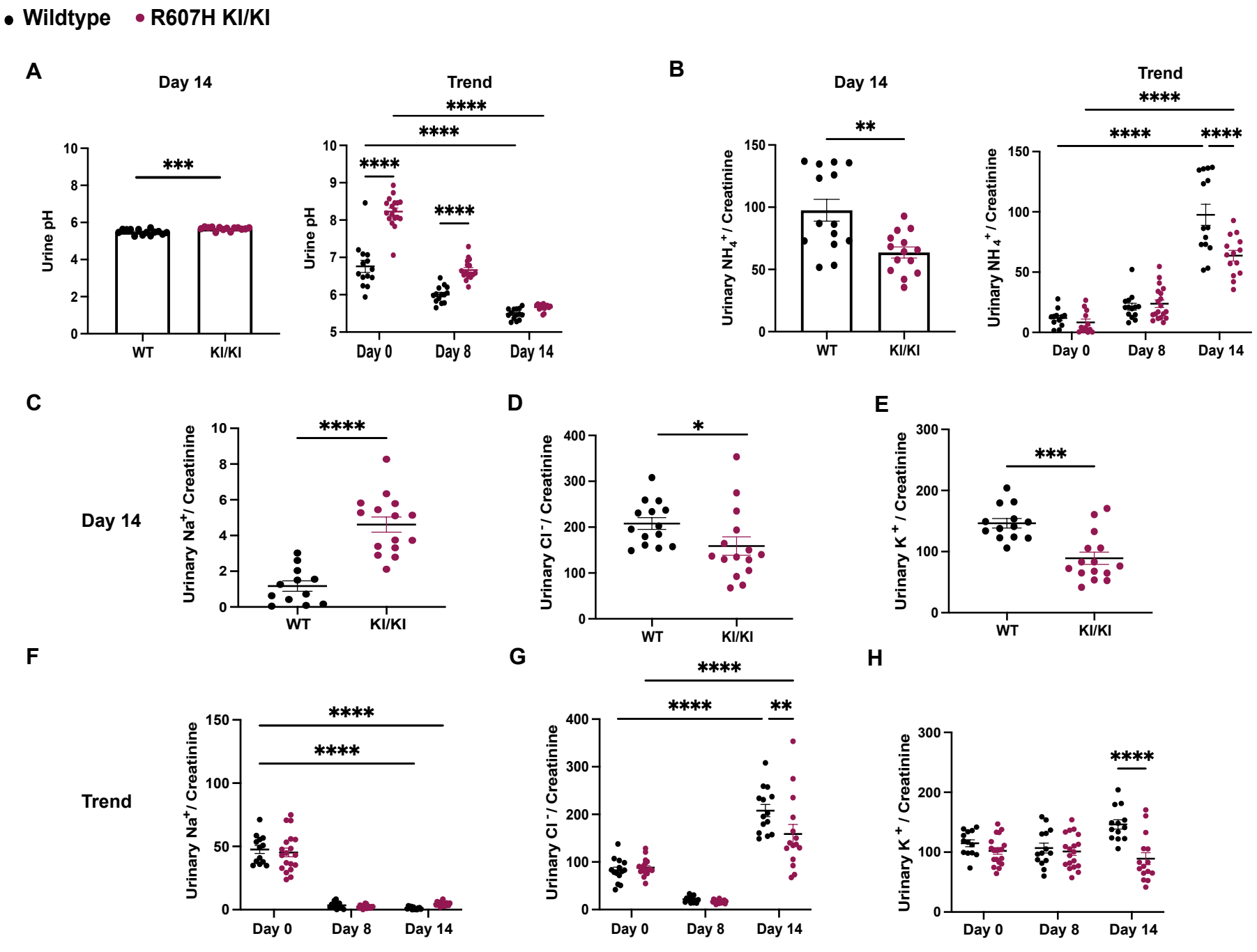

Figure 5 Mungara et al.

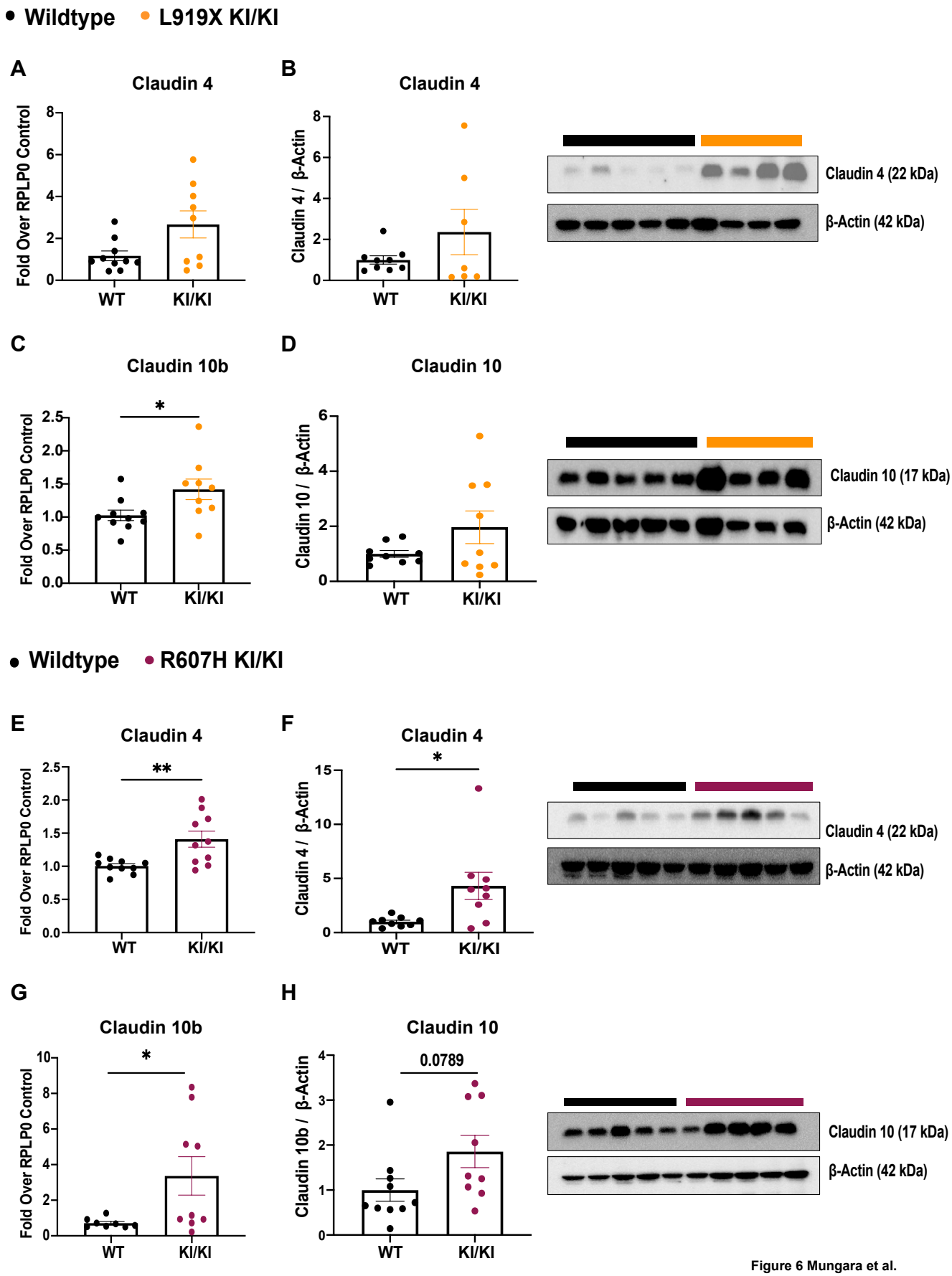

Figure 6 Mungara et al.